19

Thermal Transport in Nanostructured Materials

Aleksandr Chernatynskiy
University of Florida

David R. Clarke
Harvard University

Simon R. Phillpot
University of Florida

19.1 Introduction

A detailed understanding of thermal transport at the nanoscale is becoming increasingly needed. This need is largely being driven by two distinct technological challenges. First, continuous miniaturization of electronic devices and the ever-increasing density of the components on integrated circuits (ICs) place ever-increasing thermal loads on systems. Indeed, it is now necessary to make thermal design an integral part of the development of many electronic devices, not just at the packaging level, but also at the device and individual junction level. Moreover, as in the case of the electric conductivity, as the characteristic feature sizes ICs rapidly approach the nanoscale, the thermal transport behavior demonstrates unexpected features such as hotspots,[1] which need to be clearly understood and incorporated into complete thermal–electrical–mechanical designs. Second, ever-increasing use of the energy resources of our planet requires a realistic set of solutions that includes additional, and more efficient, ways of energy generation, energy usage, and energy distribution. Consequently, efficient energy technologies require significantly improved thermal management. In some cases, such as ICs, the primary objective is to make the thermal transport as efficient as possible. In other cases, such as thermal barrier coatings[2,3] and thermoelectric devices,[4,5] the primary objective is to minimize thermal transport. In yet other cases, such as in the case of UO_2 and other nuclear fuels, whose chemistry and microstructure evolve during burnup, the chief challenge is to understand and control the thermal environment throughout its lifetime.

The thermal conductivity of electrical insulators, from which many thermal management systems are engineered, is mediated by lattice vibrations, phonons in the language of quantum mechanics. Lattice vibrations couple to each other and can strongly couple with any structural defects—surfaces, grain boundaries, dislocations, precipitates, or point defects. As such, the thermal conductivity can be very

sensitive to microstructure; this opens up the possibility of control of thermal transport through microstructural and defect engineering. Thus, the focus of this review is the interaction of phonons with microstructure in crystalline materials and the effect on thermal transport. At very high temperatures, typically more than 1000 K, radiative contributions to the thermal conductivity can be significant; we do not address radiative transport here. We also only briefly consider thermal transport in amorphous materials.

The rest of this chapter is organized as follows. In Section 19.2, we discuss pertinent aspects of the fundamental theory of the thermal transport. Section 19.3 introduces various atomistic computational methods that are designed to overcome difficulties appearing in the theoretical approaches. The following three sections are dealing with the effects of the microstructural features on the thermal conductivity: Section 19.4 discusses point defects and other zero-dimensional features, Section 19.5 introduces dislocations contributions, while Section 19.6 probes the effects of the grain boundaries and interfaces. Section 19.7 is devoted to short overview of the thermal conductivity in the 1D structures: nanowires and nanotubes. Finally, conclusions are presented in Section 19.8.

19.2 Fundamentals of Phonon Transport

Transport of thermal energy requires carrier particles or waves that transfer energy from one region of space to another. Each of the three distinct mechanisms of thermal transport involves a different energy carrier: radiative (mediated by photons), convective (mediated by the physical movement of heat carriers), and conductive. Thermal conduction in metals is usually dominated by electrons, except in alloys with low electrical conductivity. This review focuses on thermal conduction mediated by lattice vibrations. In most electrical insulators, phonon conductivity dominates up to ~1000 K, although in some cases polaronic contributions can be significant at high temperatures.[6,7] Furthermore, heat conduction by polarons is limited to a narrow range of materials and is also particularly complicated to analyze since it is inherently a mixed electron–phonon state.

Since the theory of lattice dynamics (LD) (the theory of phonons) is well established, going back to work of Born and Huang,[8] we refer readers to a number of excellent textbooks[9,10] and reviews[11] for details. The most important aspect from the thermal transport perspective is that the motion of the individual atoms in the crystal lattice can be represented in the harmonic approximation as an ensemble of excitations, each of which has a well-defined energy and crystal momentum. The dispersion relation for the structure captures the dependence of the energy on the phonon momentum; it is typically a very complicated function determined by the intricacies of the interatomic interactions, the different types of atoms, and the crystal structure. When quantized, these excitations are referred to as phonons, a term that is often also used informally to describe classical lattice vibrations. Phonons carry energy as they propagate through the crystal and thus contribute to the thermal conductivity. Within the purely harmonic picture of lattice vibrations, phonons are the quantum eigenstates of the atomic system. Thus, they can propagate without dissipation. As a result, a purely harmonic solid has, in principle, an infinite thermal conductivity.[12] In order for a solid to have a finite thermal conductivity, as all solids actually do, dissipation must occur by phonon scattering off either each other (anharmonic interactions) or from imperfections of the lattice (point defects, dislocations, interfaces, etc.).

Treating phonons as pseudo-particles traveling through a solid, the application of basic kinetic theory easily produces an expression for the thermal conductivity, κ, known as the Debye equation:

$$\kappa = \frac{1}{3} C_v v l, \tag{19.1}$$

where

C_v is the heat capacity at constant volume

v is the velocity of the phonons, identified on this level of theory with the speed of sound

l is the phonon mean free path—the characteristic length for scattering of phonons off each other or off a structural defect

The specific heat and the speed of lattice vibrations are straightforward to determine; moreover, they are both essentially independent of the microstructure of a system. Analogous to the case in which kinetic theory is applied to gases, there is a natural interpretation of the mean free path in terms of the mean spacing between scattering events. The interpretation of the mean free path in the case of phonons can be more complicated, and most of the subsequent developments of the theory of thermal conduction, especially in crystals containing defects, are essentially based on attempts to characterize this scattering length.

Thermal transport in amorphous materials is also driven by lattice vibrations, but in a different manner.[13,14] The temperature dependences of their thermal conductivities are strikingly different: in crystalline systems, the thermal conductivity above cryogenic temperatures decreases as the temperature increases, whereas the thermal conductivity of amorphous materials above the Debye temperature increases weakly with increasing temperature. At lower temperatures, other quantum effects complicate the picture.[15] In amorphous materials, most lattice vibrations are strongly localized or have zero velocity (nonpropagating modes) and cannot contribute to the thermal conductivity in the same manner as in crystalline materials. Instead, energy transport occurs through a hopping mechanism between localized modes[14] or by "diffusion" of nonpropagating modes.[13] In the first case, anharmonicity leads to a coupling between different localized modes and an increase in the thermal transport, opposite to its effect in crystalline solid.

The formal atomistic theory of thermal conductivity incorporating defects was first worked out in detail by Klemens,[16,17] Carruthers,[18] Ziman,[19] and Callaway.[20] In their approach, the various scattering mechanisms (anharmonicity, point defects, and dislocations, for instance) are treated as perturbations to the harmonic Hamiltonian. Scattering probabilities are then computed following the Fermi Golden rule, while transport properties are described by the Boltzmann transport equation (BTE) for the probability distribution function f^{λ} of the phonons in the state λ (f_0^{λ} is the equilibrium Bose–Einstein distribution):

$$-v_{\lambda}\frac{\partial f_0^{\lambda}}{\partial T}\nabla T = \dot{f}_{scatt}^{\lambda}. \tag{19.2}$$

On the left-hand side of the equation, the usual assumption of the local equilibrium is made. Full solution of the BTE itself is a formidable task. A standard way forward is to use the relaxation time approximation (RTA). This approximation makes two assumptions: (i) if a probability distribution function for a given phonon mode is not an equilibrium distribution, then the scattering strength is proportional to the deviation from equilibrium with some characteristic time constant τ that encapsulates all the information about the scattering processes; (ii) each relaxation mode is independent of all the others, and thus, all other modes are considered to be in equilibrium. Under these assumptions, the BTE can then be simplified to

$$-v_{\lambda}\frac{\partial f_0^{\lambda}}{\partial T}\nabla T = \frac{f^{\lambda} - f_0^{\lambda}}{\tau_{\lambda}}. \tag{19.3}$$

Both assumptions can be traced to the postulated weak nonequilibrium: the first one is essentially characteristic of linear response, while the second is a direct consequence of the condition that $\Delta f = f - f_0 \ll f_0$. Equation 19.3 can also be viewed as a definition for a specific approximate perturbation Δf. Application of a variational formalism to BTE[19,21,22] shows that thermal conductivity is a functional of the perturbation from equilibrium, with the maximum value at true perturbation. From this perspective it is clear that the RTA should always underestimate the thermal conductivity. Indeed, several recent investigations[23,24] demonstrate that the RTA underestimates the thermal conductivity by as little as a few percent to about 80% in 3D solids. The general trend is that the higher the thermal conductivity

of the solid, the worse RTA performs.[24] Within the RTA, the value of the thermal conductivity can be expressed as a generalization of the Equation 19.1:

$$\kappa_{ij} = \sum_{\lambda} C_v^{\lambda} v_i^{\lambda} v_j^{\lambda} \tau_{\lambda}. \tag{19.4}$$

where

i and *j* are the Cartesian indexes

λ, as before, denotes the phonon states

This expression contains considerably more information than the simple kinetic formula, since now the contribution of each phonon state is taken into account separately, rather than using simple average values. Although still a formidable equation to evaluate, all the components in this equation can at least in principle, be calculated from the phonon properties. However, even for the simplest crystal lattices and drastically simplified atom–atom interactions, it cannot be calculated analytically. The analysis is even more difficult for complex crystal structures with realistic interatomic potentials. So, to make further progress, the Debye approximation is typically used for the phonon dispersion relationship (therefore neglecting most of the details of the true interatomic interactions). This allows the equation to be transformed from a sum over individual states to an integral over all possible phonon frequencies:

$$\kappa = \frac{1}{2\pi^2 v} \int_0^{\omega_d} C_v(\omega)\tau(\omega)\omega^2 \, d\omega. \tag{19.5}$$

With this formulation, analytic formulae can be obtained for cases in which the phonon lifetimes corresponding to different scattering mechanisms can be expressed as a function of phonon frequency. If there is more than one scattering mechanisms, the contribution of the each can then be added together by the means of the Matthiessen rule[15] to obtain the total phonon lifetime, τ.

$$\frac{1}{\tau} = \frac{1}{\tau_u} + \frac{1}{\tau_d} + \frac{1}{\tau_b} \cdots, \tag{19.6}$$

where we identify the contributions from anharmonic scattering τ_u, point defects contributions τ_d, and boundary effects τ_b. Specifically, in a perfect crystal, the contribution of the leading term of the anharmonic scattering τ_u can be expressed as[16]:

$$\frac{1}{\tau_u} = A\omega^2 T^{\xi} \exp(-B/T). \tag{19.7}$$

Integrating over the entire phonon spectrum then produces an estimate for the thermal conductivity and a dependence on 1/*T*. Since the Debye approximation is rather crude in most cases, only the functional form (temperature and frequency dependence) is claimed to be correct, while the exact numerical coefficients (*A*, *B*, and ξ in Equation 19.7) are expected to be material specific and thus have to be fitted to the experimental data. This has proven to be a reasonable approach since acoustic phonons are described surprisingly well by the Debye model and in many cases are the dominant heat carriers in simple crystal structures with only one or two atoms per unit cell (e.g., in silicon).[25] Models of this type have been widely used to fit experimental data of perfect crystalline solids. More generally, discrepancies from the anharmonic model predictions indicate that other scattering mechanisms are important. Even taking other scattering mechanisms into account, this approach lacks the power to quantitatively predict the thermal conductivity.

Theory of the kind just described allows for qualitative understanding of the lattice thermal conductivity as a function of temperature in many crystalline solids. Interplay among the three different

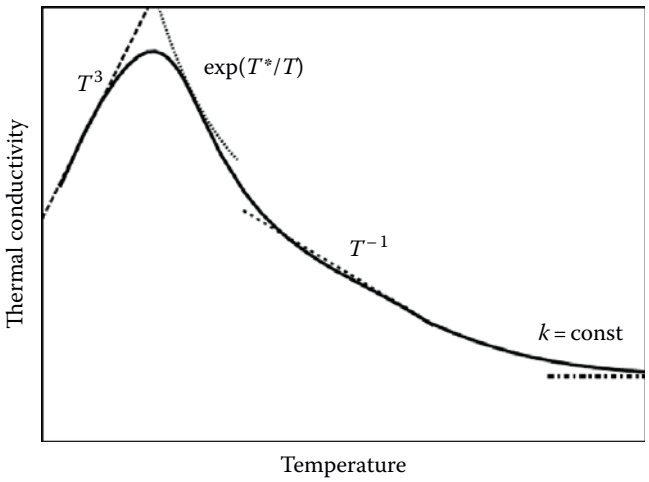

FIGURE 19.1 Generic temperature dependence of lattice thermal conductivity in a crystalline solid.

scattering mechanisms introduced in Equation 19.6 produces log–log plot in Figure 19.1.[26] At the very highest temperature, the thermal conductivity is independent of temperature. In this regime, the thermal conductivity has a minimum value, κ_{min}, as a result of the phonon mean free path being equal to the interatomic spacing.[26,27] In pure elements, this limit is rarely seen because most elements melt close to or below this temperature but it is evident in several complex oxides. As the temperature is decreased, anharmonic phonon–phonon interactions dominate and the thermal conductivity is approximately inversely proportional to temperature (experimentally observed powers are in the range of 0.9–1.3). As the temperature is lowered further, the exponential factor in τ_u starts to contribute significantly, and phonon–phonon scattering is drastically reduced. This results the thermal conductivity depending exponentially with decreasing temperature. The mean free path of the phonons ($l = v\tau$) also exponentially increases. Thus, at low (typically cryogenic) temperatures, the mean free path is limited by sample size. This effect produces a maximum in the thermal conductivity plot. The value at the maximum is therefore controlled by the samples size.[28] In nanostructured materials, this maximum is lower in magnitude and is controlled by the grain size or feature size rather than the sample size. Going back to Equation 19.4, we can see that the only temperature-dependent term left is the specific heat, which varies as T^3 at low temperature. The thermal conductivity is therefore proportional to T^3 down to cryogenic temperatures.

For complete derivations of the transport theory applied to phonons, the reader is referred to the text by Grimvall.[29] It should be emphasized that the classical $1/T$ dependence is rarely precisely given, and that rather the conductivity fits a more complex form, asymptoting at high temperatures, generally in excess of several times the Debye temperature, to a minimum value κ_{min}. Appearance of the minimum thermal conductivity might be understood from the fact that phonon mean free path in a solid cannot be smaller than the interatomic distance. Therefore, as the temperature rises and mean free path getting shorter, there ought to be a lower limit. This discussion, of course, assumes that the phonon picture of the solid is valid at these high temperatures, which is not necessarily the case. The idea of the minimum thermal conductivity[30] in disordered crystals is similar in spirit, but produced by the strong structural disorder in the system rather than thermal disorder.

The above theory provides a great deal of insight into the thermal conductivity in ideal crystalline solids. However, there are a number of examples for which the underlying approximations break down and one is forced to use computer simulations to investigate the thermal conductivity. Moreover, the RTA has been shown to be inadequate in 1D and 2D systems.[31] Furthermore, the Debye approximation that works so well for acoustic phonons does not properly describe optical phonons. These optical phonons turn out to be crucial in complex crystal structures with several different atoms per unit cell, for instance in many ionic systems, and can contribute up to about 40% of the overall thermal conductivity

in even relatively simple oxides, such as perovskite-structured $SrTiO_3$.[24] In the following section, we will discuss computational techniques for the calculation of the thermal conductivity, pointing out both their capabilities and their shortcomings.

19.3 Simulation Methods

Atomistic simulations, in contrast to the analytic methods described earlier, attempt to predict the thermal conductivity through a comprehensive and rigorous analysis of the atomic level structure and the interatomic interactions. A hierarchical classification of methods is presented in Figure 19.2 along with the relationships among them.

The most accurate descriptions of the interatomic interactions come from electronic structure methods such as density functional theory.[32] However, these methods are very computationally intensive even for basic structural and phonon analysis. As a result, their use for the analysis of thermal transport is very much in its infancy, although it can be expected to become of greater utility with continued increases in computational power. Most microscopic analysis of thermal transport properties has therefore used semi-empirical classical potentials in which the interatomic interactions are described in terms of force fields, which attempt to capture the key interatomic forces without explicitly including the electrons or their interactions. The advantages of this atomistic approach lie in its computational speed and simplicity; however, these classical potentials generally have a limited ability to faithfully represent material properties. Development of the new generation of classical potentials capable of capturing material properties in a wide variety of environments is an active area of research.[33–36] It is thus important to keep in mind that the correctness of the quantitative predictions from such methods is determined by the fidelity of the interatomic potential used in the simulations. As described in the following, other methodological limitations typically also apply.

Simulation methods for the calculation of the thermal conductivity from the atomistic perspective can be categorized as methods that compute thermal conductivity starting from the phonon properties (LD with the BTE),[21–23,37–41] methods based on nonequilibrium Green functions (NEGF),[42–44] or methods that compute thermal conductivity values directly (Green–Kubo and nonequilibrium molecular dynamics methods).[45] These methods can be viewed as complementary to each other as their ranges of applicability are quite distinct. The LD methods and the methods that start from the phonon properties are typically applicable at low temperatures (below some fraction of the melting temperature) because they correctly treat the Bose–Einstein statistics of the phonons. However, their approximate treatment of the anharmonic effects becomes increasingly indefensible as the temperature is increased. Molecular Dynamics (MD) methods, on the other hand, sample the classical atomic trajectories and are therefore strictly applicable only at high temperature (above the Debye temperature). Thus, they are most sound in the temperature region in which the phonon-based methods are the most suspect. The MD methods cannot capture the quantum effects; however, see Ref. [46] for a review of correction methods. There is also a substantial difference in the kind of systems that can be treated by the different methods. While MD methods can tackle

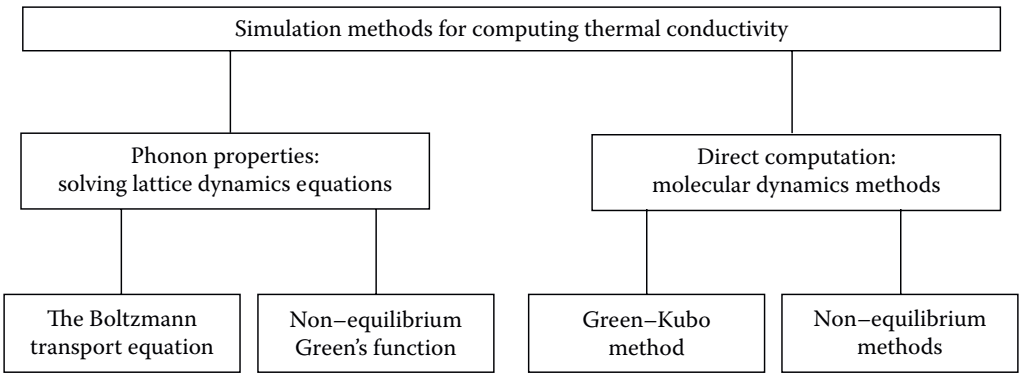

FIGURE 19.2 Relationships among atomic scale simulation methods for thermal transport.

both small and large systems, the size of the system that can be treated in LD methods is severely restricted because the computational load scales as $\sim N^4 \times k^2$, where N is the number of atoms and k is the number of k-points in the Brillouin zone.[22,41] The largest systems studied thus far are Si nanowires[47] containing up to ~3000 atoms. Here, however, only the single k-point (the Γ-point) at the center of the Brillouin zone was considered. Simulations with a realistic sampling of the k-mesh are currently restricted to far fewer atoms.

LD approaches essentially use numerical methods to work through the Klemens formulation for computing thermal conductivity as described in the previous section. That is, derivatives of an interatomic potential for a specific material are used to generate phonon dispersion relationships (from the second derivatives) and interactions among phonons (from the third derivatives, and in some cases fourth derivatives). The BTE is then linearized in the approximation of small deviations of the phonon distribution functions from equilibrium. Solution of the BTE is found either using the RTA,[41] variational method,[21,37] or by full iterative solution.[38–40] For a comparison between different methods, see Ref. [22]. One of the great advantages of this strategy is that it is possible to use first-principles calculations based on density functional theory[23,48,49] for the determination of these phonon properties. The first results of such calculations are quite encouraging, as they show very good agreement with experimental values of the thermal conductivity for Si, diamond, and Ge.[23]

Another approach that begins with phonon properties is the NEGF. This method is developed to study quantum transport in the nanostructures (for a recent review, see Ref. [50]). While the BTE method described above requires local equilibrium in the system (which essentially restricts the overall size of the system to larger than a phonon mean free path), the NEGF method does not require equilibrium to be established in the system of interest. In that sense, NEGF is the only method that is strictly valid for very small nanostructures, since the notion of the thermodynamic equilibrium for a handful of atoms is ill-defined. The premise of the method is very similar to that employed for the calculations of the electrical conductivity through molecular junctions. Namely, the nanostructure is considered to be in contact with two leads, both of which are semi-infinite and coupled to a heat bath at some temperature. Correspondingly, each of the leads has phonon populations established in them that corresponds to the lead temperature. These leads couple to a nanostructure, and heat current through the system might be expressed through the analog of Landauer formula for electrical conductivity[44]:

$$J = \frac{1}{2\pi}\int_0^\infty \mathrm{d}\omega \hbar\omega \left[f_h - f_c \right] T(\omega). \tag{19.8}$$

where

f_h and f_c are the Bose–Einstein distributions of the hot and cold leads
$T(\omega)$ is the frequency dependent transmission coefficient

The latter can be computed through the NEGF of the system, calculation of which involves the dynamical matrix of the nanostructure. Just as in the electrical case, the thermal conductivity appears to be quantized, as was indeed observed experimentally.[51] It is important to note that in contrast to the BTE approach described previously, the NEGF method is typically concerned with the ballistic transport. In that sense phonon scattering/anharmonicity of the atomic bonds is not important; rather, the thermal conductivity is a result of the quantum interference of different phonon states. However, the NEGF formalism can also be applied to a diffusive limit, well-described by the BTE.[52]

MD methods can be subdivided into nonequilibrium MD (NEMD), also known as direct methods, and Green–Kubo methods. For a comparison between the two and examples of applications see Ref. [45] and reference therein. The direct methods are very much like a simple experiment. One region of the simulation cell is heated and a second region some distance away is cooled. The temperature profile between the hot and cold regions is determined, from which the temperature gradient can be calculated. If the amount of energy needed to maintain the elevated temperature in the hot region and reduced temperature in the

cool region is known, then the heat current can be computed, from which the thermal conductivity can be calculated using Fourier's law. Thermal gradients established or defined during NEMD calculations are typically of the order 10^8–10^9 K/m, many orders of magnitude greater than the experimentally observable ones (10^2–10^3 K/m); however, Fourier's law still seems to remain valid, as demonstrated by changing the heating/cooling rate heat source/sink[45] and observing the same values of thermal conductivity.

In contrast to the NEMD method, Green–Kubo methods are based on linear response theory and compute the thermal conductivity from the heat current J correlation function:

$$\kappa_{ij} = \frac{1}{3k_B VT^2} \int_0^\infty \langle J_i(0) J_j(t) \rangle \, \mathrm{d}t. \tag{19.9}$$

Here
k_B is the Boltzmann constant
V is the volume
T is the temperature

These methods rely on intrinsic fluctuations in the energy at equilibrium without any temperature gradient. One advantage of this method is the relatively small simulation cell size required (much smaller than one required for an NEMD method) and equilibrium MD runs. The disadvantages of the Green–Kubo method include poor convergence and the intrinsic difficulty in defining the heat current for complicated many-body interatomic potentials. Both classes of MD methods also suffer from system size effects: the longest wavelength of a phonon is limited by the system size. For a detailed description of these effects and methods to take them into account see Refs. [45,53].

There are also hybrid methods for analyzing thermal transport. One method[54,55] simulates the interaction of a packet of phonons with the nanostructure (e.g., point defects,[56] grain boundaries,[57] or carbon nanotube [CN] junctions[58]). The initial state of the system of interest contains a localized wave packet of phonons from a single branch and with a narrow range of k-values. This wave packet is then allowed to propagate by evolving the system by means of standard molecular dynamics; its interaction with the nanostructure feature is then studied. Although the system is intrinsically classical, one can obtain information about the behavior of individual phonons and understand the details of the thermal transport in systems that are too large to study by the means of LD. Another approach[59,60] calculates the relaxation time of the individual phonons from equilibrium molecular dynamics (RTA-ED). The RTA is then used to calculate the thermal conductivity and provides the phonon resolution of the LD methods. Again, the use of MD simulations means that the approach is applicable only above the Debye temperature. This method does, however, have the computational advantage that they require shorter MD runs than Green–Kubo methods and smaller system sizes than direct methods.

We summarize these simulation methods in Table 19.1, which list the group of methods and the types of the approximations that are used, along with the some remarks about their capabilities.

TABLE 19.1 Comparison of Simulation Methods for Thermal Transport

Method	NEMD	GK-MD	BTE	NEGF	RTA-ED	WP
Full anharmonicity	Yes	Yes	No	No	Yes	Yes
Quantum effects	No	No	Yes	Yes	No	No
Ab initio	Yes/no	Yes/no	Yes	Yes	Yes/no	No
Low symmetry	Yes	Yes	Limited	Yes	Yes	Yes
Boundary resistance	Yes	No	No	Yes?	No	Yes

NEMD, nonequilibrium molecular dynamics; GK-MD, Green–Kubo approach; BTE, Boltzmann transport equation; NEGF, nonequilibrium Green's function method; RTA-ED, relaxation time-equilibrium dynamics; WP, Pave Packet propagation technique.

In summary, the many different tools been developed in recent years that complement each other. For each specific problem, the appropriate choice of atomistic methodology can provide reliable and rapid answers.

19.4 Point Defects and Small Clusters

We begin with a discussion of how zero-dimensional defects (point defects, precipitates, and inclusions) influence the thermal conductivity. The basic mechanism is very simple: the presence of the defect disrupts the periodicity of the lattice and provides a scattering center for phonons. This scattering can be quite strong; indeed, point defects have been shown to significantly reduce the thermal conductivity of several crystalline materials.

19.4.1 Point Defects

The simplest type of point defect is an isotopic substitution: the force constants for all of the interatomic interactions remain the same while mass is slightly altered. This case is easily treated by perturbation theory and produces additional phonon scattering with a relaxation time (as usually one resorts to Debye approximation as well)[17,61]:

$$\frac{1}{\tau_d} = V_a c_i \left(\frac{m_i - m_{ave}}{m_{ave}} \right)^2 \frac{\omega^4}{4\pi v^3}. \tag{19.10}$$

where

m_i is the mass of the isotope
c_i is its concentration
m_{ave} is the average mass of the atoms in the system
V_a is an atomic volume
v is the speed of sound

Dependence of the scattering strength on the forth power of the phonon frequency is expected in this case, since it can also be considered as Rayleigh scattering: the smallest phonon wavelength is of the order of lattice constant, while the effective size of the scattering center is the mean square displacement of the isotope atom from the lattice site (a small fraction of a lattice constant). This approach can also be extended to more than one isotope and more than one constituent atom type.[61,62]

If the defects are randomly distributed and the concentration is small, thermal conductivity is inversely proportional to the defect concentration. LD methods, using phonon properties determined from *ab initio* calculations, were used for Si, Ge, and diamond[23]; excellent agreement was obtained with the experimental data on both isotopically pure and isotopically impure samples. The effect is quite strong even for this relatively small perturbation: for example, in diamond, the difference in thermal conductivity of isotopically pure and naturally occurring samples has experimentally been found to be of the order of 40%.[63,64] Diamond is actually a very severe case because $m_i = 13$ amu, while $m_{ave} = 12$ amu. One can conclude from the studies of diamond and other simple solids that the effect of this type of simple substitution is relatively well understood.

A more complicated case is the substitution by a chemically different atom. In that case, all of the interatomic interactions, and thus the force constants, are different from the pure material. This results in contributions to the scattering beyond the isotope effect alone. Detailed calculations at the LD level are too involved in that case and one typically has to resort to the Klemens–Callaway formulation with all the detailed contributions lumped into the single "scattering strength" parameter, Γ:

$$\frac{1}{\tau_d} = \Gamma \frac{V_a \omega^4}{4\pi v^3}. \tag{19.11}$$

Klemens[17] derived formulae for the scattering parameters that involve the differences in the force constants between original atom and substitution atoms, atomic size effects, and the effect of the strain field associated with this substitution. There have been many examples of the success of this empirical approach, but it should be noted that the atomic size effects have generally been ignored in the majority of the analyses for lack of appropriate estimates of this contribution. A rather successful example of using this theory is the case of pyrochlores.[65] As yet, no calculations have been performed of this scattering parameter starting from an atomic model at the LD level. MD calculations have been performed on system with defects,[66,67] but they only yield a value for the net thermal conductivity and not any significant mechanistic insight. Simulations using the wave packet method[56] in germanium-doped silicon found that at low-defect concentrations, the scattering events are independent, the ω^4 frequency dependence predicted by Klemens holds and effect is inversely proportional to the concentration. However, if the average distance between the defects is of the order of the phonon wavelength, then this simple analysis fails. Experimental results, as well as theoretical considerations, predict that at higher concentrations their contribution changes more slowly, roughly proportional to the square root of the concentration.[68] In addition, resonant scattering effects have been observed in Si,[56] which are completely omitted from the Klemens theory but may be important in specific cases.

19.4.2 Nanoscale Precipitates and Inclusions

The effect of nanoscale precipitate and inclusions poses a particular challenge to our understanding of microstructural effects on thermal conductivity. At the largest sizes, it can be supposed that they simply act as second phases, affecting thermal conductivity through a volumetric factor, with the majority of phonons interacting with their interfaces as if they are locally planar. Under these conditions, the macroscopic effective medium theories of Nan et al.[69,70] can be expected to apply. However, when the precipitates are commensurate in size with the wavelengths of the principal components of the phonon density of states, they can be expected to further affect the thermal conductivity by altering the phonon spectrum itself. It can be argued that provided they are of atomic dimensions, they will scatter phonons in much the same way as point defects, and the Klemens–Callaway formalisms described above should be applicable. The range of validity of this assumption remains to be established since, as described earlier, the Klemens–Callaway model is a perturbation method and assumes that the scattering centers are small compared to the phonon wavelengths, and that they scatter phonons by Rayleigh scattering (an elastic scattering in the long-wavelength limit).

There are two other features of nanosized particles that have yet to be addressed satisfactorily. First, interfaces are not planar but have finite curvatures. There is presently no understanding of if, and how, curved interfaces might alter the boundary resistance (See Section 19.6 for the discussion of the boundary resistance). Second, nanosized precipitates formed by precipitation or spinodal decomposition are generally not present in dilute concentrations. Thus, the overlap of their strain fields cannot be ignored. The Klemens–Callaway model and related models treat the effects of concentration by making the matrix material an effective medium—or as Abeles describes it, a "virtual crystal"[71]—in which the scattering center is embedded.

19.4.3 Platelet Precipitates

Platelets can be formed from agglomerates of impurities, for instance *N* platelets in type Ia diamonds, or from accumulation of interstitials or vacancies produced by ion irradiation. Phonon scattering from platelet precipitates represents an intermediate case between interface scattering and spherical precipitates because of their highly anisotropic shape. Again, when the platelets are macroscopic in size, effective medium theories can adequately treat their effect on thermal conductivity.[69] However, when their dimensions approach the nanoscale, as in the case of interstitial loops and nitrogen platelets in diamond, it is not clear how best to treat their effect on thermal conductivity. Furthermore, in many practical cases, such as platelets produced by irradiation, a high concentration of point defects can be produced. Thus, assessing the effect of platelets alone is far from straightforward. Nevertheless, there is some guidance from perturbation models. For instance, the effect of thin platelets and their orientation

with respect to the heat flow direction have been considered by Turk and Klemens.[72] Simple solutions were found when the platelets were perpendicular to the phonon propagation direction for two limiting cases, one in which the platelet radius is small compared to the scattering vector, $qR < 1$, the other when the platelet radius is large compared to the scattering vector, $qR > 1$. In both limits, the scattering varies as the thickness, h, squared.[72] When $qR > 1$, an effective relaxation rate varies as $h^2R^2\omega^2$, which is the same as for an infinite sheet. In contrast, when qR is small, the scattering varies as $h^2R^4\omega^4$.

19.5 Dislocations and Other Line Defects

Understanding the effect of dislocations on the thermal conductivity is a longstanding problem and remains largely unresolved. Since the early work of Klemens[16] and others,[18,73] dislocations were recognized as possible scatterers of phonons. Three different interactions are usually invoked: (i) interaction of the incident phonons with the static strain field associated with the dislocations; (ii) a dynamic interaction by which the motion or vibration of dislocations or, at least, dislocation segments occur in response to the propagating thermoelastic strain field associated with the phonon flux. This should lead to enhanced scattering at frequencies corresponding to the dislocation segment vibrational frequencies; (iii) some form of interaction with the dislocation core since the core is characterized by differences in atomic coordination and so can be considered as a cylinder of atomic defects. In addition, in many materials, impurities segregate to dislocations and these impurities within the Cottrell atmosphere can also cause additional phonon scattering.

Following the same line of thought as discussed previously for the point defects, a number of different models have been introduced to represent these scattering mechanisms in terms of appropriate relaxation times. The contribution of the dislocation strain field was considered originally by Klemens:

$$\frac{1}{\tau_s} = \frac{2^{3/2}}{3^{7/2}} N_d b^2 \gamma^2 \omega. \tag{19.12}$$

where

N_d is the dislocation density
b is Burgers vector
γ is the Grüneisen parameter

The numerical prefactor in Equation 19.12 has different values depending on the details of the particular derivation of this contribution. This scattering mechanism predicts that the dislocation contribution to the thermal conductivity will scale as $\sim T^2$ at the cryogenic temperatures. This dependence was observed in a number of low-T experiments on various systems: Ge,[74] Cu–Ni[75] alloy, and LiF.[76] While the first two systems demonstrate a reasonable agreement with Equation 19.12, LiF shows that the effect of the dislocations is two to three orders of magnitude larger than predicted by theory, though the temperature dependence is as predicted, at least in the cryogenic temperatures.

It was suggested that in LiF, the effect of the dislocation dynamics also comes into play. On the theoretical side, models were proposed by Kneeze and Granato[77] and Ninomiya.[78] A somewhat simplified model[79] proposes the following dependence:

$$\frac{1}{\tau_d} = \frac{D}{\omega}. \tag{19.13}$$

Accounting for the dislocation motion leads to the reduction of the thermal conductivity since it is a dissipative process and leads to lower total phonon relaxation times. More complex models also have expressions for the parameter D in terms of material properties; for this reason, it was thought that this is could be a promising approach. Two different sets of experiments seem to support the theory. Thermal conductivity measurements were performed in strained LiF before and after annealing at 300 K[80] or

irradiation.[81] Both of these treatments are supposed to pin the dislocations, preventing their vibration and annealing out of the crystal. After the treatment, the strained crystals exhibited an increase of thermal conductivity almost as high as that of the unstrained crystals. Conceptual difficulties remain, however, as the theory predicts temperature dependence other than $\sim T^2$ for mobile dislocations. In addition, it is difficult to imagine dislocations moving freely in an ionic crystal at 2 K.[76] Indeed, later experiments demonstrated the energy scale of the Peierls force in LiF to be ~0.1 eV (~1000 K).[82] These pinning effects were not considered in the theory of dislocation mobility.[78] Furthermore, analysis of the Peierls stress led Ziman[19] to argue that unless the Peierls force is very weak (as in simple metals where dislocations do not dissociate significantly) even the movement of local segments of dislocations is probably unimportant in affecting thermal conductivity.

Finally, it has been proposed that the core of the dislocation itself can affect thermal conductivity, and that the effect can be expressed as

$$\frac{1}{\tau_c} = N_d \frac{r^4}{v_p^2} \omega^3. \tag{19.14}$$

where

r is a radius of the dislocation core
v_p is the phonon phase velocity

A recent investigation by Singh et al.[79] compared all three contributions and also added the effect of the stacking fault. Although satisfactory agreement for the experimental data on Ge and LiF was obtained, all the constituent parameters except the phonon frequencies in the relaxation time formulae were treated as adjustable. It is therefore difficult to judge how physically realistic the current models are. It should also be emphasized that even though few experiments have investigated the effects of dislocations on thermal conductivity, they suggest that dislocations primarily affect the conductivity at low temperatures, well below the characteristic Debye temperatures for the materials involved. It is also evident that there has been little theoretical development since the 1970s, and that several of the models do not explicitly include the Burgers vector as a parameter even though the majority of the properties of dislocations are determined by the Burgers vector.

The advent of GaN-based devices for nanostructured devices and power electronics has stimulated renewed interest in the effect of dislocations on thermal conductivity. Owing to its large electronic band gap and the recent mastery of controlling p-type doping so as to produce high-quality p–n junctions,[83,84] GaN has recently found widespread use in LEDs for displays and solid-state lighting and has growing applications in high power electronics and other applications. All these GaN devices require rapid dissipation of the heat generated during operation, and thus, a high thermal conductivity is essential. Although not as detrimental to the electronic properties as in other semiconductors, dislocations are nevertheless responsible for decreased electron mobility and nonradiative decay.[85] In principle, GaN should also have extremely high thermal conductivity on account of the low atomic number of its constituent atoms and their covalent bonding. The high value of the intrinsic thermal conductivity and the ability to grow small regions of very low dislocation densities by a variety of growth modalities, for example, lattice epitaxial overgrowth (LEO), make it of interest to investigate dislocation effects on conductivity.

Dislocations form in GaN films during growth; as a result until recently bulk, high-purity, low defect density GaN single crystals were unavailable. Consequently, the majority of GaN films are typically obtained by heteroepitaxial growth on a substrate that has a very significant mismatch (sapphire is the standard choice, with a mismatch of 17%). Despite the large mismatch, the resulting dislocation densities can be modified during growth so that regions with densities as low as 10^5 cm^{-2} can be produced while, if not optimized, the densities can be as high as 10^{10} cm^{-2} or greater. The complication is that growth is accompanied by the incorporation of impurities, such as O, Si, and Al diffusing up from the substrates and residual C and H from the growth precursors. As the growth methodologies have improved in the

last decade, the reported values of thermal conductivity have increased. Moreover, as more complete measurements of impurity and dislocation densities have been reported, there is now a clearer understanding of these two effects. At dislocation densities of $\sim 10^7$ cm^{-2} and below, the thermal conductivity of GaN at room temperature appears to be limited by impurity concentrations of $\sim 10^{18}$ cm^{-3}. At higher dislocation densities, the conductivity decreases with increasing dislocation densities. Mion et al.[86] have compiled correlations between reported thermal conductivity and dislocation densities and shown that the thermal conductivity varies as the inverse of the logarithm of the dislocation density. Much of the data was obtained from GaN materials produced with similar impurity concentrations. Together, this would indicate that the range of dislocation densities over which a dependence is observable depends on the impurity concentrations.[86] Theoretical analysis[87–89] using the original Klemens formula predicts that dislocations should only have a significant effect at densities above $\sim 10^{10}$ cm^{-2}. There is again a two to three orders of magnitude discrepancy, as in the case of LiF crystals. While it is therefore tempting to again suggest that dynamical effects might account for this discrepancy, dislocations in GaN are not mobile even at temperatures approaching the growth temperatures of ~1080°C.[90] It is thus unlikely to account for the discrepancy. Finally, recent investigations[91] used the full Callaway model to successfully fit measured thermal transport properties of a variety of GaN crystals and films, but did not discuss dislocations in detail.

Although we have focused in this section on the role of dislocations on the thermal conductivity, it is important to emphasize that the active junctions, where heat is generated, in modern electronic and optical devices are all at the nanometer length scale. The heat has then to be dissipated by conduction over longer length scales; consequently, the thermal properties at both the nanoscale and the mesoscale, where there can be large variations in dislocation densities are important. While the recent work on GaN has clarified the role of dislocation density, the effect of the other dislocation parameters, such as Burgers vector and dislocation line orientation, still needs to be understood.

19.6 Grain Boundaries and Interfaces

19.6.1 Interface Thermal Resistance

A key aspect of thermal transport in many nanomaterials is the presence of a very high density of interfaces and grain boundaries. These interfaces present additional phonon scattering features that have few well-defined characteristics. In general, though, one can consider that they produce a temperature jump ΔT at the interface, with a magnitude that is characterized by an interfacial (Kapitza) conductance, G_k:

$$J = G_k \Delta T, \tag{19.15}$$

where J is the heat current. This is the analog of Fourier's law. The inverse of the conductance, $R = 1/G_k$, is known as a Kapitza resistance. Originally, the term "Kapitza resistance" was applied only to solid/liquid interfaces at cryogenic temperatures,[92] but it is now widely used to apply to solid/solid interfaces as well. In spite of 70 years of study of interfacial thermal transport, a detailed microscopic description of the Kapitza resistance is still lacking. However, a number of useful models have been proposed. The two most widely used, the acoustic mismatch model (AMM)[93] and the diffusive mismatch model (DMM)[94] are elastic models, in the sense that a phonon of a specific frequency incident on the interface can produce only the phonon of the same frequency on other side of the interface.

The AMM essentially assumes that continuity and continuum mechanics are valid, and that interfaces are flat and ideal, that they have no intrinsic properties of their own but simply delineate regions with different elastic properties. Directly analogous to optics, sound waves are reflected or transmitted through the interface depending on the incident angle and the acoustic impedances (analogous to the refractive indexes) of the solids. Hence the AMM works well for the long-wavelength acoustic phonons near the center of the Brillouin zone. At low temperatures, these are the only phonon states that

are occupied and the AMM works particularly well. In this model, the transmittance of an interface between two dissimilar materials, A and B, each having different acoustic impedances, Z, is given by

$$t = \frac{4Z_A Z_B}{\left(Z_A + Z_B\right)^2}. \tag{19.16}$$

As with plane wave acoustics and optics, similar relationships can be developed to account for polarization and angles of incidence.

The basic assumption of the DMM is essentially the converse of the assumption in the AMM: upon arriving at an interface a phonon scatters diffusively, and completely loses memory of where it came from. The probability for transmission or reflection is then determined by the phonon densities of states of the materials on either side of the interface. The DMM is typically able to describe the Kapitza resistance at room temperature and above, but inconsistencies still remain. Possible origins of these inconsistencies include neglect of the inelastic processes[95] and disregard of the interface structure, as well as the presence of the heat carriers other than phonons (e.g., electrons in metals). It is interesting to note that while the assumptions in the AMM and DMM models are dramatically different, there is no trend in the values of the predicted interfacial resistances for solid–solid interfaces between the models: sometimes the AMM value is larger than the DMM value, sometimes it is smaller.[94]

Many real interfaces, including grain boundaries and especially interfaces between dissimilar materials, are neither flat nor atomically abrupt, nor even crystallographically coherent. Furthermore, in nanosized polycrystalline materials, the interfaces have very large curvatures. This would suggest that the DMM might be the more appropriate model but this remains a subject for intensive study. There have been some attempts to incorporate interface structural and chemical disorder in calculations of thermal conductance; for example, Beechem et al.[96] uses an effective medium approximation to represent the interface within the DMM. The phonon-hopping model introduced by Braginsky et al.[97] treats thermal transport in granular materials assuming that scattering from the grain boundaries is the principal mechanism that limits thermal conductivity. One of the main results of their model is an expression for the Kapitza resistance and its temperature dependence. When applied to cubic zirconia, the Kapitza resistance is consistent with the measurements from cryogenic to room temperature.[98]

19.6.2 Grain-Size Effects

Historically, the first investigations of possible size effects on thermal conductivity were those devoted to determining grain size effects in polycrystalline materials. Among the first were studies of the effect of grain size of SiGe alloys[99–101] on their thermoelectric properties. These showed a significant but relatively small effect, in large part because the grain sizes were quite large and the areal density of grain boundaries correspondingly small. More significant grain size effects have since been reported. For instance, Bhattacharya et al.[102] showed that the room temperature thermal conductivity of a shock compacted sample of Sb-doped TiNiSn half-Heusler alloys decreases with grain size below about 10–20 μm, falling from well above 10 W/mK to as low as 3.7 W/mK. While there were clearly grain size effects, any interpretation was complicated since the materials were not fully dense and the shock compaction presumably resulted in a very high density of dislocations. A clearer dependence on grain size was found in the work by Yang et al.[98] who studied nanocrystalline, yttria-stabilized cubic zirconia films produced by metal organic chemical vapor deposition (MOCVD). These studies indicated a very strong grain size effect over the range of ~10–100 nm at both cryogenic temperatures (25 K) and up to 480 K, the latter very close to the reported Debye temperature (475 K). More recently, these results have been extended but using fully dense, transparent bulk yttria-stabilized tetragonal zirconia to larger grain sizes of about 0.2 μm.[103]

The effect of grain size can be modeled by introducing a relaxation time associated with grain boundary scattering. Assuming purely elastic scattering, the relaxation time is related to the grain size, d, by

$$\tau_{gb} = \frac{d}{v_s}, \tag{19.17}$$

where v_s is the speed of sound. The overall thermal conductivity is then given by the argument that the grain boundaries are thermal resistors in series with the grains resulting in an expression of the form:

$$\kappa = \frac{\kappa_i}{1 + \dfrac{R_k \kappa_i}{d}}, \tag{19.18}$$

where

κ_i is the intrinsic conductivity of the material in the grains
R_k is the Kapitza resistance of the grains[69]

In analyzing the effect of grain size on the thermal conductivity of nanocrystalline materials, the concept of the Kapitza length is useful. The Kapitza length, l_k, is defined as the thickness of the material of thermal conductivity κ that provides the same change in temperature as a given interface[70]:

$$l_k = \frac{\kappa}{G_k}. \tag{19.19}$$

If the grain size is much larger then Kapitza length, $d > l_k$, then the granularity of the material should not significantly affect the thermal conductivity of the polycrystal. Conversely, when the size of the grains approaches the Kapitza length, boundary scattering becomes significant and will reduce the thermal conductivity below that of large grain material as suggested by Equation 19.18. Characteristic values of the Kapitza length are ~50 nm in Si at 1000 K,[104] and ~10 nm for UO_2 value at 1000 K.[105]

Ultra-nanocrystalline diamond is a very sensitive system in which to study the grain size effect, owing to a long mean free path of the heat carrying phonons. In particular, thermal conductivity can be reduced by the two orders of magnitude for the grain size of ~0.1 μm.[106] At the same time, measurements found unusually high boundary conductance, ~3000 MW/m^{2}K, for diamond grain boundaries[107]: this is about 10 times larger than typical range of the of the Kapitza conductance of 20–200 MW/m^{2}K. However, when recast in terms of the Kapitza length (about 750 nm), this value is not at all unusual and is compatible with other interfaces. Molecular dynamics simulations using Tersoff potential for carbon found the values of boundary conductance in good agreement with experiment, and demonstrated, that boundary conductance in diamond grain boundaries depends very weakly on the type of the boundary.[104]

The temperature dependence of the thermal conductivity of nanocrystalline materials is of interest for many applications. Within the RTA, the overall relaxation time is

$$\frac{1}{\tau} = \frac{1}{\tau_u} + \frac{1}{\tau_d} + \frac{1}{\tau_{gb}} \cdots \tag{19.20}$$

Evaluation of this formula using values obtained from large grain material for the intrinsic thermal conductivity of the grains indicates that not only does the thermal conductivity decrease with increasing temperature but also that the grain size dependence becomes less pronounced until, at the highest temperatures, there is no apparent grain size effect on thermal conductivity. This is illustrated for the case of yttria-stabilized, tetragonal zirconia in Figure 19.3. The implication is that the clear benefits of nanocrystalline material in reducing thermal conductivity at room temperature and below are not realizable at very high temperatures.

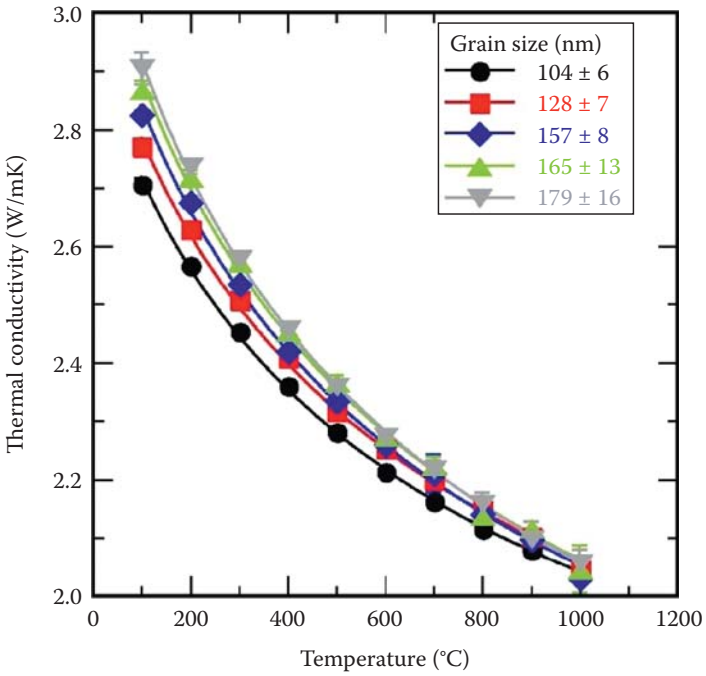

FIGURE 19.3 Thermal conductivity as a function of temperature for tetragonal zirconia stabilized with 3 m/o yttria for samples aged by grain growth at 1200°C to the sizes indicated. (From Limarga, A. and Clarke, D.R., *Appl. Phys. Lett.*, 98(21), 211906, 2011.)

While the experimental studies of Yang et al.[98] and Limarga and Clarke[103] combined with Equation 19.18 clearly indicate that the Kapitza resistance is temperature dependent up to the Debye temperature, and becomes temperature independent as the temperature is increased, they do not unfortunately provide any insight into the physical origin of the Kapitza resistance or the effects of boundary curvature on the Kapitza resistance.

19.6.3 Synthetic Superlattices

The clearest and most unambiguous nanoscale effects on thermal conductivity come from studies of the thermal conductivity of synthetic superlattices, that is, periodic, 1D structures formed by deposition techniques, including molecular beam epitaxy (MBE) and electron-beam deposition. By careful control of the deposition parameters, well-defined superlattice periodicities and compositions can be produced. Within this category, superlattices with coherent and incoherent interfaces can be produced, and in some cases, the superlattices are repeating amorphous and crystalline layers of material, for example, W/amorphous alumina.[108] In such a structure, the thermal conductivity is controlled by the transition from coherent to incoherent thermal transport[109]: At very small periods of the superlattice (just a few atomic layers), the system behaves as a monolithic bulk structure with a large unit cell. As the period increases, the unit cell becomes larger and larger, which leads to a decrease in the thermal conductivity as a function of the layer thickness. This can also be understood as folding of the phonon bands as the size of the crystallographic unit cell increases, along with the appearance of the gaps in the phonon spectra. These effects lead to the flattening of the phonon bands and therefore, reduction of the phonon group velocities, which results in lower thermal conductivity. However, as the period length increases above a few nanometers, a superlattice starts to behave as an interfacial system, meaning that the overall thermal conductivity now is the combination of the bulk thermal conductivities of the superlattice constituents (typically quite large) in series with the interface boundary conductance. In this regime, fewer interfaces means larger thermal conductivity; therefore, an increase in period length leads to an increase in the thermal conductivity, approaching that of single crystal

material. There is a certain period length, where the thermal conductivity has a minimum value.[109–111] This minimum value been measured to be lower than the random alloy limit for the AlN/GaN[112] and Bi_2Te_3/Sb_2Te_3.[111] Such superlattices therefore have a potential in thermoelectric applications. While a minimum in thermal conductivity is consistently observed in numerical MD studies, it is not always in experiment. MD simulations by Daly et al.[113] show that this disagreement may be due to the roughness of the interfaces: disorder at the interface leads to a monotonic reduction of the thermal conductivity as the superlattice period is reduced.

19.6.4 Natural Superlattices

Many complex oxides are, in effect, naturally occurring superlattices, since their unit cells can be thought of as consisting of the stacking of two or more blocks with different crystal structures. Perhaps, the best known are the Ruddlesden–Popper phases,[114,115] the Aurivillius phases,[116–118] and the Dion–Jacobson phases,[119] see Table 19.2. Not only do these families of phases often have interesting properties, ferroelectricity for example, but the superlattice periodicity can be systematically changed by altering the composition. The major feature of these natural superlattices as compared to synthetic superlattices is that the interfaces are inherently coherent. This enables a clean study to be made of the effects of superlattice spacing on thermal conductivity. The measurements made so far indicate that these structures could be invaluable for the study of phonon scattering in periodic structures.

A number of natural superlattice compounds have been studied to date, and all of them have rather low thermal conductivities, with the lowest values being parallel to the stacking direction, that is, perpendicular to the interfaces between the blocks. An example is bismuth titanate, $Bi_4Ti_3O_{12}$, an Aurivillius phase consisting of alternating blocks of pseudoperovskite structure $(Bi_2Ti_3O_2)^{2-}$ and fluorite $(Bi_2O_2)^{2+}$ structure.[120] Interestingly, not only is the thermal conductivity crystallographically anisotropic but the thermal conductivity along the *c*-axis, that is, across the interfaces, is temperature independent up to 1000°C (see Figure 19.4). Measurements also indicate that the conductivity remains constant down to at least 150 K. At this stage, the origin of this temperature independence is not clear, but suggestive of being due to the predominance of interface phonon scattering.

The thermal conductivity of the Sr–Ti–O Ruddlesden–Popper phases has also been studied by MD.[121] These phases consist of a repeated stacking of a block of perovskite coordinated layers and rock salt layers. The MD results demonstrate that the thermal conductivity along the stacking direction exhibits a minimum as a function of the number of perovskite layers in the perovskite block (Figure 19.5). The simulations also show that the in-plane conductivity does not exhibit an obvious minimum.

TABLE 19.2 Ruddlesden–Popper, Dion–Jacobson, and Aurivillius Phases Composition and Structure

Ruddlesden–Popper	Dion–Jacobson	Aurivillius
$A'_2[A_{n-1}B_nX_{3n+1}]$	$M^{+1}A_{(n-1)}B_nO_{(3n+1)}$	$(Bi_2O_2)[A_{n-1}B_nX_{3n+1}]$
	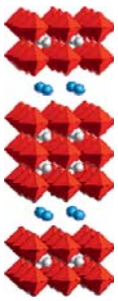	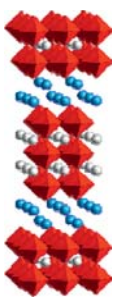

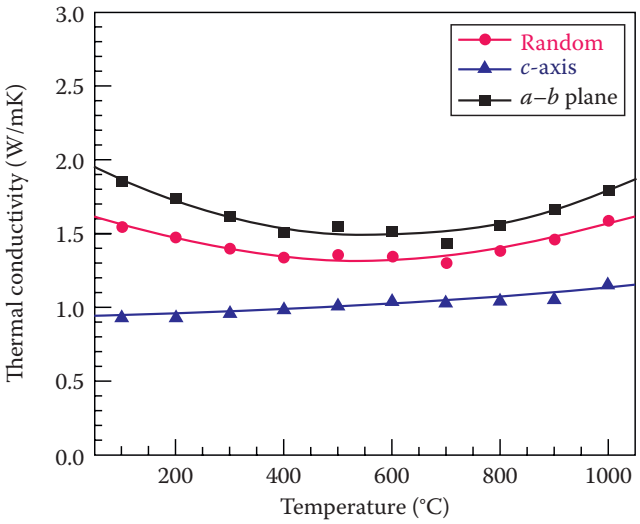

FIGURE 19.4 Thermal conductivity in $Bi_4Ti_3O_{12}$ along different crystallographic directions.

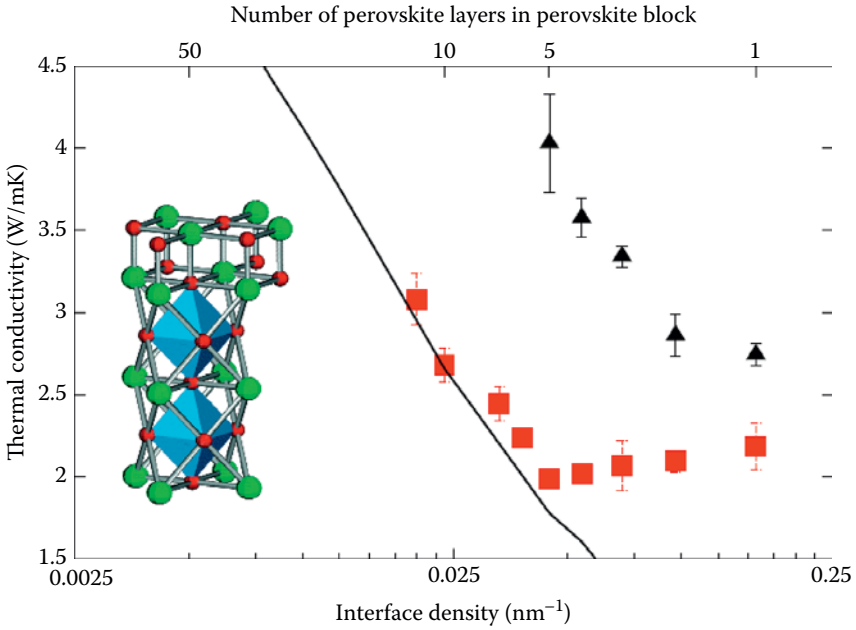

FIGURE 19.5 Thermal conductivity in Ruddlesden–Popper phases of Sr–Ti–O system as a function of the interface density. (From Chernatynskiy, A. et al., *Appl. Phys. Lett.*, 95(16), 161906-1, 2009.)

From the results in Figure 19.5, one can deduce the boundary conductance introduced by the rock salt layers starting from the thicknesses of only two perovskites layers (Figure 19.6) from the temperature profile obtained in direct method MD simulations. This boundary conductance for a thin perovskites layers is thickness dependent, indicating that the system is in the coherent regime and that the phonon properties of the interface are intimately tied with those of the perovskites block. This behavior is in accord with the experimental findings in the synthetic superlattice system AlN/GaN,[122] where similar dependence of the boundary conductance on the layers thickness was measured. However, at a thickness of about 10 perovskite cells, the interfacial conductance saturates: at this point, the phonons in the system are essentially phonons in the perovskite block that scatter off the interface between the perovskite and rock salt layers.

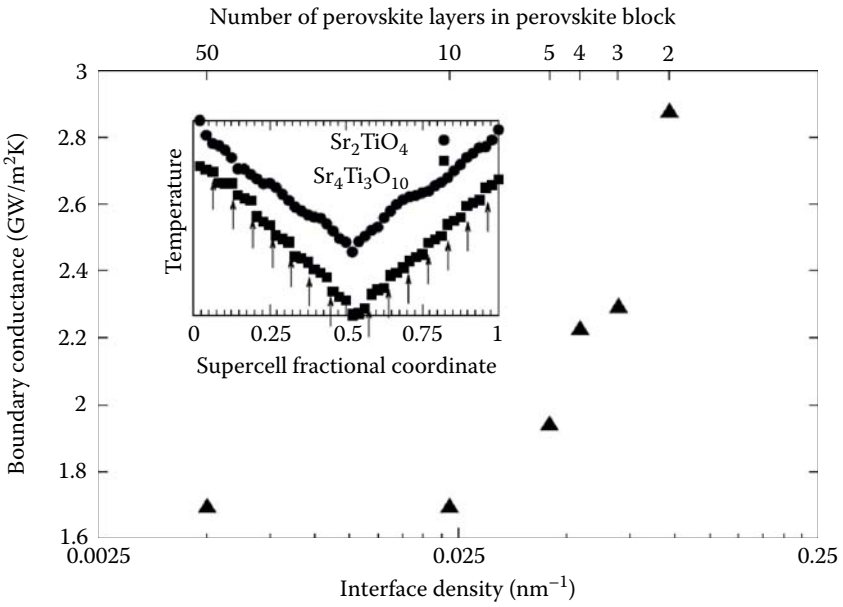

FIGURE 19.6 Boundary thermal conductance of the SrO layers as a function of the perovskite thickness. Inset: jumps in the temperature profile, characteristic of the boundary thermal conductance.

19.7 Nanotubes and Nanowires

The tremendous interest in nanowires and the possibility of making semiconductor device structures by altering composition and dopant concentration during growth to produce 1D modulations provides the first opportunity to compare thermal conductivity models for 1D structures with experiment. The thermal conductivity of individual silicon nanowires was the first to be measured.[123] This demonstrated a significant reduction in the thermal conductivity, compared to bulk silicon, as well as strong nanowire radius dependence, indicative of the importance of boundary scattering. The simplest approximation is to assume that phonon scattering occurs from the walls of the nanowires and so, just as in nanograined materials, the phonon lifetime varies proportionally to the nanowire diameter. The thermal conductivity is then reduced compared to the bulk value and scales linearly with the diameter. However, the experimental decrease[123] is significantly greater than predicted by this simple model. Rough nanowires show yet a stronger decrease.[124] From the perspective of the atomistic simulations,[47] it was also demonstrated that surface roughness is one the key components of the low thermal conductivity. In particular, for silicon nanowires, the combination of the boundary scattering and low thermal conductivity of the amorphous silicon oxide layer that always forms on the surface is the main driver for the reduction in the thermal conductivity. While providing atomic resolution for the nanowire structure, these studies were also limited to very thin nanowires: 1–4 nm range of diameters,[47] which is small compared to the smallest, 22 nm diameter used in the experiments. To tackle larger nanowires, a number of models been developed that take into account the phonon scattering of the rough interface.[125–127] One such model[127] treats the rough interface as a space varying dilation of the wire. The relaxation time associated with this scattering mechanism can be computed with the help of the perturbation theory since the roughness of the surface is the only input parameter (other than phonon properties of the bulk material) required. Results of the application of this model reproduce experimental findings quite successfully for the silicon nanowires, and moreover, predict that roughness-limited thermal conductivity should scale as a square of the diameter. However, in these analyses, the surface roughness is treated as parameter because accurate determination of the nanowire surface roughness from the experimental data is currently unavailable. Further reduction of the thermal conductivity is possible through the standard vehicle of alloying with Ge.[128,129] Interestingly

enough, in that case, the diameter dependence is not nearly as strong as in the case of the pure silicon nanowires, indicating that the alloy scattering was is the dominant scattering mechanism. However, it is also possible that the nanowire sizes were not sufficiently small to enter the roughness-limited regime. A related problem occurs in predicting the electrical conductivity of nanowires and interconnects as their cross-sectional size is reduced.[130] For more details, the reader is referred to a recent review on the subject.[131]

The contribution from the amorphous layer/surface roughness also explain the results of the nanowires thermal conductivity measurements in other semiconductors, such as GaN,[132] CdS,[133] lead halcogenates,[134] and PdTe[135] are smaller than that of the bulk materials but not anywhere as dramatic as in the case of silicon. All these compounds form well-defined single crystalline nanowires, hence the boundary scattering alone is responsible for reduction in the thermal conductivity.

Nanotubes are also 1D systems. CNs are most often considered, though the thermal properties of the B-N and B-C-N nanotubes have also been measured.[136] There are two reasons to believe that nanotubes should have exceptionally high thermal conductivities. First, the carbon–carbon bond is highly harmonic in nature. Second, the structure of the CNs is very different from that of the nanowires: while nanowires might be considered as a small piece of bulk material, for which boundary resistance and associated effects are important and affect thermal transport significantly, a CN is a rolled-up sheet of graphene, seamlessly connected such that there are no boundaries, except possibly at its ends.

Nanotubes are also unique systems because they are probably the closest experimental representations of truly 1D systems. While one can consider polymers as another example of 1D systems, it is very difficult to make suspended polymers, free of interactions with a supporting substrate. Truly 1D systems would have qualitatively different transport properties from a 3D system: in particular, Fourier's law is not valid and thermal conductivity (defined in terms of heat current) is dependent of the length of the 1D object.[137,138] Such a dependence was indeed observed experimentally.[139] Here, one has to distinguish between ballistic transport and anomalous 1D transport. The former is a result of the mean free path of particular phonons being longer than the system size; in this case, the apparent thermal conductivity with the system size up to some length, but then saturates. This is somewhat analogous to the dependence of the thermal conductivity on the sample size in 3D case at cryogenic temperatures and was proposed as an explanation for the inconsistent results of the thermal conductivity of CN in the literature.[51,140] Anomalous transport, by contrast, is an intrinsic property of the 1D system; in that case, the thermal conductivity scales with some power length, typically 2/5.[137] An interesting explanation for this behavior was recently proposed in the context of polymers: Henry and Chen[141] argued that the phonon–phonon scattering events in 1D systems are rare compared to the 3D bulk, and therefore, they can be correlated in some way. This argument also explains why calculation of the thermal conductivity of the CN with the BTE technique[140] provides asymptotically length-independent results: the BTE assumes that all scattering events are independent of each other. Complete resolution of this question is still missing, however.

The thermal conductivity of an individual suspended CN is about 3000 W/mK at room temperature[142]; this is very high and attractive for applications. One possible route for utilizing this high thermal conductivity is to form composite materials with randomly dispersed nanotube fibers acting as an enhancer for the overall thermal conductivity. Weak interactions of the CN with the surroundings allow it to preserve relatively high thermal conductivity: CN bundles demonstrate a reduction of the thermal conductivity by a factor of 2 when compared with individual CN,[143] while the thermal of immersed/filled with liquid CN is reduced by 20%–35%.[144] However, this weak interaction also implies a very low boundary conductance between CN and the matrix material, which in turn have very strong negative effect on the overall composite thermal conductivity.[145,146] Composites formed of only CN also have thermal conductivities significantly lower than individual CN. For example, thermal conductivities of 2D nanotube arrangements (buckypaper) are about ~75 W/mK.[147] Moreover, upon transition to the random 3D network structure, thermal conductivity reduces to miniscule ~0.13–0.2 W/mK.[148] Low volume fraction and the large number of interconnects with poor boundary conductance are the reasons for such poor performance.

19.8 Concluding Remarks

Lattice thermal conductivity remains a significant challenge for material science. While the basic understanding of the thermal transport mechanisms was developed in the 1950s and 1960s, their manifestation in particular material structures and for particular crystallographies continue to be worked out. In this chapter, we have tried to illustrate how current algorithms and increased computational power are beginning to yield a much deeper understanding of the effects of the micro- and nanostructuring on thermal conductivity. An overview of the computational methods that allow achieving that understanding and examples of their applications was also presented.

In spite of the great strides made, a large number of open questions remain. From the theoretical perspective, the problem can be partitioned into several components. Any method for the calculation of the thermal conductivity will only be as good as the underlying interatomic potential is. Use of first-principles calculations is an example of an area in which progress continues to be made and will have high impact. At the same time, the development of semi-empirical methodologies that can reproduce thermal conductivity with good precision is very important as well. LD methods and molecular dynamics methods can be viewed as complementary methodologies (LD takes account of the quantum nature of the phonons, but fails to describe anharmonicity correctly, while MD is just the opposite); therefore, both of these techniques will be applied extensively. While first-principles MD is possible and been demonstrated as a proof of principle for the thermal conductivity calculations, it is not expected to being routinely used for this purpose in the near future. It thus seems likely that classical potentials will remain the driving force for the MD studies of the thermal transport.

Improvement in the methodologies is the next challenge. LD techniques are not only limited in the way they represent anharmonicity, but also in scaling with the system size. Development of multiscale methods and/or appropriate approximations to improve the scaling are important research directions. Both Green–Kubo and direct methods molecular dynamics simulations also suffer from size effects associated with the simulation supercell, which are still not fully understood.

As far as the understanding of the effect of the particular nanoscale microstructural features is concerned, very little is known about how particular atomic arrangements of atoms in the nanostructure affect thermal transport in the system. The interface boundary resistance is an excellent example of this kind of problem: MD is essentially the only method that can simulate the boundary resistance, though its insight into interface structure influence is somewhat limited. The situation is quite similar with the dislocations: the dislocation core structure is produced by atomic relaxations that are very sensitive to the interatomic interactions. Thermal transport in the 1D structures is an exciting new direction of the research with the possible applications in thermoelectric and heat management.

In conclusion, the engineering of the thermal transport properties of nanostructures is of ever-increasing importance. While great strides have been made, a large number of critical issues remain unresolved.

Acknowledgments

This work was supported by the NSF Materials World Network Project under Grant No. DMR-0710523. This work was coauthored by a subcontractor (SRP) of the U.S. Government under DOE Contract No. DE-AC07-05ID14517, under the Energy Frontier Research Center (Office of Science, Office of Basic Energy Science, FWP 1356). Accordingly, the U.S. Government retains and the publisher (by accepting the article for publication) acknowledges that the U.S. Government retains a nonexclusive, paid-up, irrevocable, worldwide license to publish or reproduce the published form of this manuscript, or allow others to do so, for U.S. Government purposes.

References

1. E. Pop and K. E. Goodson, Thermal phenomena in nanoscale transistors, *J. Electron. Packaging*, 128(2), 102–108 (2006).
2. C. G. Levi, Emerging materials and processes for thermal barrier systems, *Curr. Opin. Solid State Mater. Sci*., 8(1), 77–91 (2004).
3. D. R. Clarke and S. R. Phillpot, Thermal barrier coating materials, *Mater. Today*, 8(6), 22–29 (2005).
4. D. Rowe, ed., *Thermoelectrics Handbook: Macro to Nano*. CRC Press, Boca Raton, FL (2005).
5. G. A. Slack, *New Materials and Performance Limits for Thermoelectric Cooling*, pp. 407–440. CRC Press, Boca Raton, FL (1995).
6. J. Harding and D. Martin, A recommendation for the thermal conductivity of UO_2, *J. Nucl. Mater*., 166(3), 223–226 (1989).
7. J. M. Casado, J. H. Harding, and G. J. Hyland, Small-polaron hopping in Mott-insulating UO_2, *J. Phys. Condens. Matter*, 6(25), 4685 (1994).
8. M. Born and K. Huang, *Dynamical Theory of Crystal Lattices*. Oxford University Press, Oxford, UK (1954).
9. N. W. Ashcroft and N. D. Mermin, *Solid State Physics*. Brooks Cole, Belmont, CA (1976).
10. G. Venkataraman, F. A. Feldkamp, and V. C. Sahnim, *Dynamics of the Perfect Crystals*. The MIT Press, Cambridge, MA (1975).
11. C.-L. Tien, A. Majumdar, and G. Gerner, eds., *Microscale Energy Transport*. Taylor & Francis, New York, NY (1997).
12. R. Peierls, Zur Theorie der galvanomagnetischen Effekte, *Ann. Physik*, 3, 1055 (1929).
13. P. B. Allen and J. L. Feldman, Thermal conductivity of disordered harmonic solids, *Phys. Rev. B*, 48(17), 12581–12588 (1993).
14. H. Böttger and T. Damker, Hopping theory of heat transport in disordered systems, *Phys. Rev. B*, 50(17), 12509–12519 (1994).
15. R. Berman, *Thermal Conduction in Solids*. Clarendon Press, Oxford, U.K. (1976).
16. P. G. Klemens, Thermal conductivity and lattice vibrational modes, *Solid State Phys*., 7, 1–98 (1958).
17. P. G. Klemens, The scattering of low-frequency lattice waves by static imperfections, *Proc. Phys. Soc. A*, 68(12), 1113 (1955).
18. P. Carruthers, Theory of thermal conductivity of solids at low temperatures, *Rev. Mod. Phys*., 33(1), 92 (1961).
19. J. Ziman, *Electrons and Phonons*. Clarendon Press, Oxford, U.K. (1962).
20. J. Callaway, Model for lattice thermal conductivity at low temperatures, *Phys. Rev*., 113(4), 1046–1051 (1959).
21. S. Pettersson, Solving the phonon Boltzmann equation with the variational method, *Phys. Rev. B*, 43(11), 9238–9246 (1991).
22. A. Chernatynskiy and S. R. Phillpot, Evaluation of computational techniques for solving the Boltzmann transport equation for lattice thermal conductivity calculations, *Phys. Rev. B*, 82(13), 134301 (2010).
23. A. Ward, D. A. Broido, D. A. Stewart, and G. Deinzer, Ab initio theory of the lattice thermal conductivity in diamond, *Phys. Rev. B*, 80(12), 125203 (2009).
24. A. Chernatynskiy, J. Turner, A. J. McGaughey, C. Amon, and S. Phillpot, Phonon mediated thermal conductivity in ionic solids by lattice dynamics based methods, *J. Am. Ceram. Soc*., 94, 3523–3531 (2011).
25. A. S. Henry and G. Chen, Spectral phonon transport properties of silicon based on molecular dynamics simulations and lattice dynamics, *J. Comput. Theor. Nanosci*., 5, 141–152(12) (2008).
26. D. Clarke, Materials selection guidelines for low thermal conductivity thermal barrier coatings, *Surf. Coat. Technol*., 163, 67–74 (2003).
27. M. Roufosse and P. Klemens, Lattice thermal-conductivity of minerals at high-temperatures, *J. Geophys. Res*., 79(5), 703–705 (1974).

28. R. Berman, E. L. Foster, and J. M. Ziman, Thermal conduction in artificial sapphire crystals at low temperatures .1. Nearly perfect crystals, *Proc. Roy. Soc. A*, 231, 130 (1955).
29. G. Grimvall, *Thermophysical Properties of Materials*. North Holland, Amsterdam, the Netherlands (1986).
30. D. G. Cahill, S. K. Watson, and R. O. Pohl, Lower limit to the thermal conductivity of disordered crystals, *Phys. Rev. B*, 46(10), 6131–6140 (1992).
31. L. Lindsay, D. A. Broido, and N. Mingo, Lattice thermal conductivity of single-walled carbon nanotubes: Beyond the relaxation time approximation and phonon–phonon scattering selection rules, *Phys. Rev. B*, 80(12), 125407 (2009).
32. P. Parr and W. Yang, *Density-Functional Theory of Atoms and Molecules*. Oxford University Press, New York (1989).
33. M. S. Daw and M. I. Baskes, Embedded-atom method: Derivation and application to impurities, surfaces, and other defects in metals, *Phys. Rev. B*, 29(12), 6443–6453 (1984).
34. A. C. T. van Duin, S. Dasgupta, F. Lorant, and W. A. Goddard, ReaxFF: A reactive force field for hydrocarbons, *J. Phys. Chem. A*, 105(41), 9396–9409 (2001).
35. D. W. Brenner, O. A. Shenderova, J. A. Harrison, S. J. Stuart, B. Ni, and S. B. Sinnott, A second-generation reactive empirical bond order (REBO) potential energy expression for hydrocarbons, *J. Phys. Condens. Matter*, 14(4), 783 (2002).
36. T.-R. Shan, B. D. Devine, J. M. Hawkins, A. Asthagiri, S. R. Phillpot, and S. B. Sinnott, Second-generation charge-optimized many-body potential for Si/SiO_2 and amorphous silica, *Phys. Rev. B*, 82(23), 235302 (2010).
37. S. Pettersson, Calculation of the thermal conductivity of alkali halide crystals, *J. Phys. C Solid State*, 20(8), 1047 (1987).
38. M. Omini and A. Sparavigna, Beyond the isotropic-model approximation in the theory of thermal conductivity, *Phys. Rev. B*, 53(14), 9064–9073 (1996).
39. M. Omini and A. Sparavigna, Heat transport in dielectric solids with diamond structure, *Nuovo Cimento D*, 19(10), 1537–1563 (1997).
40. D. A. Broido, A. Ward, and N. Mingo, Lattice thermal conductivity of silicon from empirical interatomic potentials, *Phys. Rev. B*, 72(1), 014308 (2005).
41. J. E. Turney, E. S. Landry, A. J. H. McGaughey, and C. H. Amon, Predicting phonon properties and thermal conductivity from anharmonic lattice dynamics calculations and molecular dynamics simulations, *Phys. Rev. B*, 79(6), 064301 (2009).
42. N. Mingo and L. Yang, Phonon transport in nanowires coated with an amorphous material: An atomistic Green's function approach, *Phys. Rev. B*, 68(24), 245406 (2003).
43. J.-S. Wang, J. Wang, and N. Zeng, Nonequilibrium Green's function approach to mesoscopic thermal transport, *Phys. Rev. B*, 74(3), 033408 (2006).
44. T. Yamamoto and K. Watanabe, Nonequilibrium Green's function approach to phonon transport in defective carbon nanotubes, *Phys. Rev. Lett.*, 96(25), 255503 (2006).
45. P. K. Schelling, S. R. Phillpot, and P. Keblinski, Comparison of atomic-level simulation methods for computing thermal conductivity, *Phys. Rev. B*, 65(14), 144306 (2002).
46. J. E. Turney, A. J. H. McGaughey, and C. H. Amon, Assessing the applicability of quantum corrections to classical thermal conductivity predictions, *Phys. Rev. B*, 79(22), 224305 (2009).
47. D. Donadio and G. Galli, Atomistic simulations of heat transport in silicon nanowires, *Phys. Rev. Lett.*, 102(19), 195901 (2009).
48. X. Tang and J. Dong, Lattice thermal conductivity of MgO at conditions of Earth's interior, *Proc. Natl. Acad. Sci. USA*, 107(10), 4539–4543 (2010).
49. J. Garg, N. Bonini, B. Kozinsky, and N. Marzari, Role of disorder and anharmonicity in the thermal conductivity of silicon–germanium alloys: A first-principles study, *Phys. Rev. Lett.*, 106(4), 045901 (2011).
50. J.-S. Wang, J. Wang, and J. T. Lü, Quantum thermal transport in nanostructures, *Eur. Phys. J. B*, 62(4), 381–404 (2008).

51. K. Schwab, E. Henriksen, J. Worlock, and M. Roukes, Measurement of the quantum of thermal conductance, *Nature*, 404(6781), 974–977 (2000).
52. Y. Xu, J.-S. Wang, W. Duan, B.-L. Gu, and B. Li, Nonequilibrium Green's function method for phonon–phonon interactions and ballistic-diffusive thermal transport, *Phys. Rev. B*, 78(22), 224303 (2008).
53. D. P. Sellan, E. S. Landry, J. E. Turney, A. J. H. McGaughey, and C. H. Amon, Size effects in molecular dynamics thermal conductivity predictions, *Phys. Rev. B*, 81(21), 214305 (2010).
54. P. K. Schelling, S. R. Phillpot, and P. Keblinski, Phonon wave-packet dynamics at semiconductor interfaces by molecular-dynamics simulation, *Appl. Phys. Lett*., 80(14), 2484–2486 (2002).
55. C. Kimmer, S. Aubry, A. Skye, and P. K. Schelling, Scattering of phonons from a high-energy grain boundary in silicon: Dependence on angle of incidence, *Phys. Rev. B*, 75(14), 144105 (2007).
56. M. Yao, T. Watanabe, P. K. Schelling, P. Keblinski, D. G. Cahill, and S. R. Phillpot, Phonon-defect scattering in doped silicon by molecular dynamics simulation, *J. Appl. Phys*., 104(2), 024905 (2008).
57. P. K. Schelling, S. R. Phillpot, and P. Keblinski, Kapitza conductance and phonon scattering at grain boundaries by simulation, *J. Appl. Phys*., 95(11), 6082–6091 (2004).
58. V. Varshney, J. Lee, A. K. Roy, and B. L. Farmer, Modeling of interface thermal conductance in longitudinally connected carbon nanotube junctions, *J. Appl. Phys*., 109(8), 084913 (2011).
59. A. J. C. Ladd, B. Moran, and W. G. Hoover, Lattice thermal conductivity: A comparison of molecular dynamics and anharmonic lattice dynamics, *Phys. Rev. B*, 34(8), 5058–5064 (1986).
60. J. A. Thomas, J. E. Turney, R. M. Iutzi, C. H. Amon, and A. J. H. McGaughey, Predicting phonon dispersion relations and lifetimes from the spectral energy density, *Phys. Rev. B*, 81(8), 081411 (2010).
61. D. T. Morelli, J. P. Heremans, and G. A. Slack, Estimation of the isotope effect on the lattice thermal conductivity of group IV and group III–V semiconductors, *Phys. Rev. B*, 66(19), 195304 (2002).
62. R. Berman, E. l. Foster, and J. Ziman, The thermal conductivity of dielectric crystals—The effect of isotopes, *Proc. Roy. Soc. A*, 237(1210), 344–354 (1956).
63. D. G. Onn, A. Witek, Y. Z. Qiu, T. R. Anthony, and W. F. Banholzer, Some aspects of the thermal conductivity of isotopically enriched diamond single crystals, *Phys. Rev. Lett*., 68(18), 2806–2809 (1992).
64. J. R. Olson, R. O. Pohl, J. W. Vandersande, A. Zoltan, T. R. Anthony, and W. F. Banholzer, Thermal conductivity of diamond between 170 and 1200 K and the isotope effect, *Phys. Rev. B*, 47(22), 14850–14856 (1993).
65. C. L. Wan, W. Pan, Q. Xu, Y. X. Qin, J. D. Wang, Z. X. Qu, and M. H. Fang, Effect of point defects on the thermal transport properties of $(La_xGd_{1-x})_2Zr_2O_7$: Experiment and theoretical model, *Phys. Rev. B*, 74(14), 144109 (2006).
66. G. Paolini, P. Lindan, and J. Harding, The thermal conductivity of defective crystals, *J. Chem. Phys*., 106(9), 3681–3687 (1997).
67. T. Watanabe, S. G. Srivilliputhur, P. K. Schelling, J. S. Tulenko, S. B. Sinnott, and S. R. Phillpot, Thermal transport in off-stoichiometric uranium dioxide by atomic level simulation, *J. Am. Ceram. Soc*., 92(4), 850–856 (2009).
68. F. L. Vook, Change in thermal conductivity upon low-temperature electron irradiation: GaAs, *Phys. Rev*., 135(6A), A1742–A1749 (1964).
69. C. W. Nan, R. Birringer, D. R. Clarke, and H. Gleiter, Effective thermal conductivity of particulate composites with interfacial thermal resistance, *J. Appl. Phys*., 81(10), 6692–6699 (1997).
70. C. W. Nan and R. Birringer, Determining the Kapitza resistance and the thermal conductivity of polycrystals: A simple model, *Phys. Rev*., 57(14), 8264–8268 (1998).
71. B. Abeles, Lattice thermal conductivity of disordered semiconductor alloys at high temperatures, *Phys. Rev*., 131(5), 1906–1911 (1963).
72. L. A. Turk and P. G. Klemens, Phonon scattering by impurity platelet precipitates in diamond, *Phys. Rev*., 9(10), 4422–4428 (1974).
73. K. Ohashi, Scattering of lattice waves by dislocations, *J. Phys. Soc. Jpn*., 24(3), 437–445 (1968).

74. M. Sato and K. Sumino, Effect of dislocations on the low temperature thermal conductivity in germanium, *J. Phys. Soc. Jpn*., 36(4), 1075–1083 (1974).
75. M. Kusunoki and H. Suzuki, Lattice thermal conductivity of deformed copper–aluminum alloy crystals at low temperatures, *J. Phys. Soc. Jpn*., 26(4), 932–938 (1969).
76. R. L. Sproull, M. Moss, and H. Weinstock, Effect of dislocations on the thermal conductivity of lithium fluoride, *J. Appl. Phys*., 30(3), 334–337 (1959).
77. G. A. Kneeze and A. V. Granato, Effect of independent and coupled vibrations of dislocations on low-temperature thermal conductivity in alkali halides, *Phys. Rev. B*, 25(4), 2851–2866 (1982).
78. T. Ninomiya, Dislocation vibration and phonon scattering, *J. Phys. Soc. Jpn*., 25(3), 830–840 (1968).
79. B. K. Singh, V. J. Menon, and K. C. Sood, Phonon conductivity of plastically deformed crystals: Role of stacking faults and dislocations, *Phys. Rev. B*, 74(18), 184302 (2006).
80. T. Suzuki and H. Suzuki, Effect of dislocations on the thermal conductivity of LiF, *J. Phys. Soc. Jpn*., 32(1), 164–171 (1972).
81. A. C. Anderson and M. E. Malinowski, Interaction between thermal phonons and dislocations in LiF, *Phys. Rev. B*, 5(8), 3199–3210 (1972).
82. T. Suzuki and H. Kim, Low-temperature deformation and dislocation mechanism in LiF, *J. Phys. Soc. Jpn*., 39(6), 1566–1571 (1975).
83. M. Shur and R. Davis eds., *GaN Based Materials and Devices*. World Scientific Publishing Co, New Jersey, NJ (2004).
84. S. Nakamura, *Nitride Semiconductor Blue Lasers and Light Emitting Diodes*. CRC Press, Boca Raton, FL (2000).
85. S. Bennett, Dislocations and their reduction in GaN, *Mater. Sci. Technol*., 26, 1017–1028(12) (2010).
86. C. Mion, J. F. Muth, E. A. Preble, and D. Hanser, Accurate dependence of gallium nitride thermal conductivity on dislocation density, *Appl. Phys. Lett*., 89(9), 092123 (2006).
87. J. Zou, D. Kotchetkov, A. A. Balandin, D. I. Florescu, and F. H. Pollak, Thermal conductivity of GaN films: Effects of impurities and dislocations, *J. Appl. Phys*., 92(5), 2534–2539 (2002).
88. D. Kotchetkov, J. Zou, A. A. Balandin, D. I. Florescu, and F. H. Pollak, Effect of dislocations on thermal conductivity of GaN layers, *Appl. Phys. Lett*., 79(26), 4316–4318 (2001).
89. X.-G. Yu and X.-G. Liang, Effect of isotope on lattice thermal conductivity of lateral epitaxial overgrown GaN, *Diamond Relat. Mater*., 16(9), 1711–1715 (2007).
90. L. Sugiura, Dislocation motion in GaN light-emitting devices and its effect on device lifetime, *J. Appl. Phys*., 81(4), 1633–1638 (1997).
91. A. AlShaikhi, S. Barman, and G. P. Srivastava, Theory of the lattice thermal conductivity in bulk and films of GaN, *Phys. Rev. B*, 81(19), 195320 (2010).
92. P. Kapitza, The study of heat transfer in Helium II, *Zh. Eksp. Teor. Fiz*., 11, 1 (1941).
93. I. M. Khalatnikov, Teploobmen mezhdu tverdym telom i geliem-ii, *Zh. Eksp. Teor. Fiz*., 22(6), 687–704 (1952).
94. E. T. Swartz and R. O. Pohl, Thermal boundary resistance, *Rev. Mod. Phys*., 61(3), 605–668 (1989).
95. P. E. Hopkins, J. C. Duda, and P. M. Norris, Anharmonic phonon interactions at interfaces and contributions to thermal boundary conductance, *J. Heat Transf*., 133(6), 062401 (2011).
96. T. Beechem, S. Graham, P. Hopkins, and P. Norris, Role of interface disorder on thermal boundary conductance using a virtual crystal approach, *Appl. Phys. Lett*., 90, 054104 (2007).
97. L. Braginsky, V. Shklover, H. Hofmann, and P. Bowen, High temperature phonon thermal conductivity of nanostructures, *Phys. Rev. B*, 70, 134201 (2004).
98. H. Yang, G. R. Bai, L. J. Thompson, and J. A. Eastman, Interfacial thermal resistance in nanocrystalline yttria-stabilized zirconia, *Acta Mater*., 50, 2309–2317 (2002).
99. N. Savvides and H. J. Goldsmid, Boundary scattering of phonons in fine grained hot-pressed Ge–Si alloys: I. The dependence of lattice thermal conductivity on grain size and porosity, *J. Phys. C Solid State*, 13, 4657–4670 (1980).

100. D. M. Rowe and V. S. Shukla, The effect of phonon-grain boundary scattering on the lattice thermal conductivity and thermoelectric conversion efficiency of heavily doped fine-grained, hot-pressed silicon germanium alloy, *J. Appl. Phys*., 52, 7421 (1981).
101. N. Savvides and H. J. Goldsmid, Boundary scattering of phonons in fine-grained hot-pressed Ge–Si alloys: II. Theory, *J. Phys. C Solid State*, 13, 4671–4678 (1980).
102. S. Bhattacharya, T. M. Tritt, Y. Xia, V. Ponnambalam, S. J. Poon, and N. Thadhani, Grain size effects on the lattice thermal conductivity of Ti-based half-Heusler alloys, *Appl. Phys. Lett*., 81(1), 43–45 (2002).
103. A. Limarga and D. R. Clarke, The grain size and temperature dependence of the thermal conductivity of polycrystalline, tetragonal yttria-stabilized zirconia, *Appl. Phys. Lett.,* 98(21), 211906 (2011).
104. T. Watanabe, Thermal transport in uranium dioxide and diamond by atomic level simulations. PhD thesis, University of Florida, Gainesville, FL (2008).
105. T. Watanabe, S. B. Sinnott, J. S. Tulenko, R. W. Grimes, P. K. Schelling, and S. R. Phillpot, Thermal transport properties of uranium dioxide by molecular dynamics simulations, *J. Nucl. Mater*., 375(3), 388–396 (2008).
106. J. E. Graebner, V. G. Ralchenko, A. A. Smolin, E. D. Obraztsova, K. G. Korotushenko, and V. I. Konov, Thermal conductivity of thin diamond films grown from d.c. discharge, *Diamond Relat. Mater*., 5(6–8), 693–698 (1996). *Proceedings of the 6th European Conference on Diamond, Diamond-like and Related Materials*, held in Barcelona, Part 2.
107. M. A. Angadi, T. Watanabe, A. Bodapati, X. Xiao, O. Auciello, J. A. Carlisle, J. A. Eastman, P. Keblinski, P. K. Schelling, and S. R. Phillpot, Thermal transport and grain boundary conductance in ultrananocrystalline diamond thin films, *J. Appl. Phys*., 99(11), 114301 (2006).
108. R. M. Costescu, D. G. Cahill, F. H. Fabreguette, Z. A. Sechrist, and S. M. George, Ultra-low thermal conductivity in W/Al_2O_3 nanolaminates, *Science*, 303, 989–990 (2004).
109. M. V. Simkin and G. D. Mahan, Minimum thermal conductivity of superlattices, *Phys. Rev. Lett*., 84(5), 927–930 (2000).
110. Z. Chen, J. Yang, P. Zhuang, M. Chen, J. Zhu, and Y. Chen, Thermal conductivity measurement of InGaAs/InGaAsP superlattice thin films, *Chinese Sci. Bull*., 51, 2931–2936 (2006). doi: 10.1007/s11434-006-2208-8
111. R. Venkatasubramanian, Lattice thermal conductivity reduction and phonon localization-like behavior in superlattice structures, *Phys. Rev. B*, 61(4), 3091–3097 (2000).
112. W. S. Capinski, H. J. Maris, T. Ruf, M. Cardona, K. Ploog, and D. S. Katzer, Thermal-conductivity measurements of GaAs/AlAs superlattices using a picosecond optical pump-and-probe technique, *Phys. Rev. B*, 59(12), 8105–8113 (1999).
113. B. C. Daly, H. J. Maris, K. Imamura, and S. Tamura, Molecular dynamics calculation of the thermal conductivity of superlattices, *Phys. Rev. B*, 66(2), 024301 (2002).
114. S. N. Ruddlesden and P. Popper, New compounds of the K_2NiF_4 type, *Acta Crystallogr*., 10(8), 538–540 (1957).
115. S. N. Ruddlesden and P. Popper, The compound $Sr_3Ti_2O_7$ and its structure, *Acta Crystallogr*., 11(1), 54–55 (1958).
116. B. Aurivillius, Mixed bismuth oxides with layer lattices. 1. The structure type of $Canb_2Bi_2O_9$, *Arkiv for Kemi*, 1(5), 463–480 (1950).
117. B. Aurivillius, Mixed oxides with layer lattices .3. Structure of $BaBi_4Ti_4O_{15}$, *Arkiv for Kemi*, 2(6), 519–527 (1951).
118. B. Aurivillius, The structure of Bi_2NbO_5F and isomorphous compounds, *Arkiv for Kemi*, 5(1), 39–47 (1953).
119. M. Dion, M. Ganne, and M. Tournoux, Nouvelle familles de phases a feuillets 'perovskites', *Mater. Res. Bull*., 16(11), 1429–1435 (1981).
120. Y. Shen, D. R. Clarke, and P. A. Fuierer, Anisotropic thermal conductivity of the Aurivillius phase, bismuth titanate ($Bi_4Ti_3O_{12}$): A natural nanostructured superlattice, *Appl. Phys. Lett*., 93(10), 102907 (2008).

121. A. Chernatynskiy, R. W. Grimes, M. A. Zurbuchen, D. R. Clarke, and S. R. Phillpot, Crossover in thermal transport properties of natural, perovskite-structured superlattices, *Appl. Phys. Lett*., 95(16), 161906-1, (2009).
122. Y. K. Koh, Y. Cao, D. G. Cahill, and D. Jena, Heat-transport mechanisms in superlattices, *Adv. Funct. Mater*., 19(4), 610–615 (2009).
123. D. Li, Y. Wu, P. Kim, L. Shi, P. Yang, and A. Majumdar, Thermal conductivity of individual silicon nanowires, *Appl. Phys. Lett*., 83(14), 2934–2936 (2003).
124. A. I. Hochbaum, R. Chen, R. D. Delgado, W. Liang, E. C. Garnett, M. Najarian, A. Majumdar, and P. Yang, Enhanced thermoelectric performance of rough silicon nanowires, *Nature*, 451(7175), 163–167 (2008).
125. N. Mingo, L. Yang, D. Li, and A. Majumdar, Predicting the thermal conductivity of Si and Ge nanowires, *Nano Lett.*, 3(12), 1713–1716 (2003).
126. M. Kazan, G. Guisbiers, S. Pereira, M. R. Correia, P. Masri, A. Bruyant, S. Volz, and P. Royer, Thermal conductivity of silicon bulk and nanowires: Effects of isotopic composition, phonon confinement, and surface roughness, *J. Appl. Phys*., 107(8), 083503 (2010).
127. P. Martin, Z. Aksamija, E. Pop, and U. Ravaioli, Impact of phonon-surface roughness scattering on thermal conductivity of thin Si nanowires, *Phys. Rev. Lett*., 102(12), 125503 (2009).
128. M. K. Y. Chan, J. Reed, D. Donadio, T. Mueller, Y. S. Meng, G. Galli, and G. Ceder, Cluster expansion and optimization of thermal conductivity in SiGe nanowires, *Phys. Rev. B*, 81(17), 174303 (2010).
129. H. Kim, I. Kim, H. jin Choi, and W. Kim, Thermal conductivities of Si[sub 1 – x]Ge[sub x] nanowires with different germanium concentrations and diameters, *Appl. Phys. Lett*., 96(23), 233106 (2010).
130. W. Steinhögl, G. Schindler, G. Steinlesberger, and M. Engelhardt, Size-dependent resistivity of metallic wires in the mesoscopic range, *Phys. Rev. B*, 66(7), 075414 (2002).
131. R. Rurali, Colloquium: Structural, electronic, and transport properties of silicon nanowires, *Rev. Mod. Phys*., 82(1), 427–449 (2010).
132. T. Westover, R. Jones, J. Y. Huang, G. Wang, E. Lai, and A. A. Talin, Photoluminescence, thermal transport, and breakdown in Joule-heated GaN nanowires, *Nano Lett*., 9(1), 257–263 (2009).
133. X. F. Liu, R. Wang, Y. P. Jiang, Q. Zhang, X. Y. Shan, and X. H. Qiu, Thermal conductivity measurement of individual CdS nanowires using microphotoluminescence spectroscopy, *J. Appl. Phys*., 108(5), 054310 (2010).
134. M. Fardy, A. I. Hochbaum, J. Goldberger, M. M. Zhang, and P. Yang, Synthesis and thermoelectrical characterization of lead chalcogenide nanowires, *Adv. Mater*., 19(19), 3047 (2007).
135. J. W. Roh, S. Y. Jang, J. Kang, S. Lee, J.-S. Noh, W. Kim, J. Park, and W. Lee, Size-dependent thermal conductivity of individual single-crystalline PbTe nanowires, *Appl. Phys. Lett*., 96(10), 103101 (2010).
136. C. W. Chang, W.-Q. Han, and A. Zettl, Thermal conductivity of B–C–N and BN nanotubes, *Appl. Phys. Lett*., 86(17), 173102 (2005).
137. S. Lepri, R. Livi, and A. Politi, Thermal conduction in classical low-dimensional lattices, *Phys. Rep*., 377(1), 1–80 (2003).
138. Z. Liu and B. Li, Heat conduction in a one-dimensional harmonic chain with three-dimensional vibrations, *J. Phys. Soc. Jpn*., 77(7), 074003 (2008).
139. C. W. Chang, D. Okawa, H. Garcia, A. Majumdar, and A. Zettl, Breakdown of Fourier's law in nanotube thermal conductors, *Phys. Rev. Lett*., 101(7), 075903 (2008).
140. N. Mingo and D. A. Broido, Length dependence of carbon nanotube thermal conductivity and the problem of long waves, *Nano Lett*., 5(7), 1221–1225 (2005). PMID: 16178214.
141. A. Henry and G. Chen, Anomalous heat conduction in polyethylene chains: Theory and molecular dynamics simulations, *Phys. Rev. B*, 79(14), 144305 (2009).
142. P. Kim, L. Shi, A. Majumdar, and P. L. McEuen, Thermal transport measurements of individual multiwalled nanotubes, *Phys. Rev. Lett*., 87(21), 215502 (2001).

143. J. Che, T. Cagin, and W. A. Goddard. III, Thermal conductivity of carbon nanotubes, *Nanotechnology*, 11(2), 65 (2000).
144. J. A. Thomas, R. M. Iutzi, and A. J. H. McGaughey, Thermal conductivity and phonon transport in empty and water-filled carbon nanotubes, *Phys. Rev. B*, 81(4), 045413 (2010).
145. S. Shenogin, L. Xue, R. Ozisik, P. Keblinski, and D. Cahill, Role of thermal boundary resistance on the heat flow in carbon-nanotube composites, *J. Appl. Phys*., 95(12), 8136–8144 (2004).
146. S. Huxtable, D. Cahill, S. Shenogin, L. Xue, R. Ozisik, P. Barone, M. Usrey et al. Interfacial heat flow in carbon nanotube suspensions, *Nat. Mater*., 2(11), 731–734 (2003).
147. M. E. Itkis, F. Borondics, A. Yu, and R. C. Haddon, Thermal conductivity measurements of semitransparent single-walled carbon nanotube films by a bolometric technique, *Nano Lett*., 7(4), 900–904 (2007).
148. R. S. Prasher, X. J. Hu, Y. Chalopin, N. Mingo, K. Lofgreen, S. Volz, F. Cleri, and P. Keblinski, Turning carbon nanotubes from exceptional heat conductors into insulators, *Phys. Rev. Lett*., 102(10), 105901 (2009).